IOP Conference Series:
Earth and
Environmental Science

PAPER • OPEN ACCESS

The Earth Climate Observatory space mission concept for the monitoring of the Earth Energy Imbalance

To cite this article: S. Dewitte *et al* 2025 *IOP Conf. Ser.: Earth Environ. Sci.* **1522** 012019

The Earth Climate Observatory space mission concept for the monitoring of the Earth Energy Imbalance

S. Dewitte[1], T. Mauritsen[2], B. Meyssignac[3], T. August[4], L. Schifano[4], L. Smeesters[5], R. Roca[3], H. Brindley[6], J. Russell[6], N. Clerbaux[7], R. Hollmann[8], L. Megner[2], M. Haberreiter[9], J. Gumbel[2], J. Marotzke[10], J. Riedi[11], A. Riihelä[12], T. Trent[13], M. Wendisch[14]

[1] Royal Observatory of Belgium, Brussels, Belgium

[2] Stockholm University, Stockholm, Sweden

[3] Laboratoire d'études en Géophysique et Océanographie Spatiales, Toulouse, France

[4] European Space Agency, Noordwijk, Netherlands

[5] Vrije Universiteit Brussel, Brussels, Belgium

[6] Imperial College, London, UK

[7] Royal Meteorological Insitute of Belgium, Brussels, Belgium

[8] Deutscher Wetterdienst, Offenbach, Germany

[9] Physical-Meteorological Observatory and World Radiation Center, Davos, Switzerland

[10] Max Planck Institute for Meteorology, Hamburg, Germany

[11] Lille University, Lille, France

[12] Finnish Meteorological Institute, Helsinki, Finland

[13] Earth Observation Science/National Centre for Earth Observation, School of Physics & Astronomy, University of Leicester, Leicester, UK

[14] Leipzig University, Leipzig, Germany

E-mail: steven.dewitte@oma.be

Abstract. We present the Earth Climate Observatory space mission concept - currently studied in Phase 0 as a European Space Agency Earth Explorer 12 candidate - for the measurement of the Earth Energy Imbalance and the Earth Radiation Budget. Key innovations are 1) the differential Sun-Earth observation with identically constructed wide field of view radiometers, 2) an adequate sampling of the seasonal diurnal cycle with a constellation of polar precessing orbits, 3) complementary full angular coverage at high spatial resolution using wide field of view multispectral cameras.

IOP Conf. Series: Earth and Environmental Science **1522** (2025) 012019 doi:10.1088/1755-1315/1522/1/012019

1 Mission Justification

Monitoring the Earth Energy Imbalance (EEI) is of prime importance for a predictive understanding of climate change [Hansen et al., 2005], [Von Schuckmann et al., 2016]. Furthermore, monitoring of the EEI gives an early indication on how well mankind is doing in implementing the Paris Climate Agreement [UN, 2016].

Monitoring Earth's global mean radiation balance is essential because the surplus in this energy causes global warming, sea level rise and extreme weather around the globe [IPCC, 2021]. As the governments of the world have agreed to limit global warming to below 2 degrees in the Paris Climate Agreement [UN, 2016], it is essential to have a system in place that can monitor progress towards reaching the goal, warn against possible fast warming if aerosol induced cooling is underestimated, and also to avert a low-probability but catastrophic global instability tipping point in time.

EEI is defined as the small difference between the incoming energy the Earth receives from the Sun and the outgoing energy lost by Earth to space. Both the incoming solar and the terrestrial outgoing energy are of the order of 340 W/m^2 at the global annual mean level [Dewitte and Clerbaux, 2017], while the EEI is of the order of 0.9 W/m^2 [Trenberth et al., 2016], [Von Schuckmann et al., 2020]. The EEI is cumulated in the Earth climate system, particularly in the oceans, due to their substantial heat capacity, and results in global temperature rise.

Currently the best estimates of the absolute value of the EEI [Trenberth et al., 2016], [Von Schuckmann et al., 2020], and of its long term variation [Minière et al., 2023] are obtained from in situ observations, with a dominant contribution of the time derivative of the Ocean Heat Content (OHC). These in situ EEI observations can only be made over long time periods, typically a decade or longer. In contrast, with direct observations of the EEI from space, in principle the EEI can be measured at the annual mean time scale. However, the EEI is currently poorly measured from space, due to two fundamental challenges.

The first fundamental challenge is that the EEI is the difference between two opposing terms of nearly equal amplitude. Currently, the incoming solar radiation and outgoing terrestrial radiation are measured with separate instruments, which means that their calibration errors are added and overwhelm the signal to be measured. The current error on the direct measurement of the EEI is of the order of 5 W/m^2 [Dewitte and Clerbaux, 2017], significantly larger than the signal to be measured of the order of 1 W/m^2. To make significant progress in this challenge, a **differential** measurement using **identical intercalibrated instruments** to measure both the incoming solar radiation and the outgoing terrestrial radiation is needed [Mishchenko et al., 2016].

The second fundamental challenge is that the outgoing terrestrial radiation has a systematic diurnal cycle. Current observations of the outgoing terrestrial radiation is sampled from the so-called morning and afternoon Sun-synchronous orbits, complemented by narrow band geostationary imagers [Doelling et al., 2013], [Loeb et al., 2018]. Recently the sampling from the morning orbit was abandoned [Kato et al., 2023]. The sampling of the diurnal cycle can be improved, for example, by using **two orthogonal 90° inclined orbits** [Hocking et al., 2024] which give both **global coverage**, and a **statistical sampling of the full diurnal cycle** at seasonal (3 months) time scale. Other alternatives being investigated are orbits with 82 or 73-degree inclinations, which precess to obtain better sampling of the diurnal and annual cycles but require filling in the polar caps. A complementary Sun-synchronous orbit would provide synergies with several other systems.

For understanding the radiative forcing – e.g. aerosol radiative forcing [Kaufman et al., 2005],[Alfaro-Contreras et al., 2017] - and climate feedback – e.g. ice albedo feedback [Hartmann and Ceppi, 2014],[Dewitte et al., 2019] - mechanisms underlying changes in the EEI, and for climate model validation, it is necessary to separate the Total Outgoing Radiation (TOR) spectrally into the two compenents of the Earth Radiation Budget (ERB), namely the Reflected Solar radiation (RSR) and Outgoing Longwave Radiation (OLR) and to map them at relatively high spatial resolution. To intercalibrate the high-accuracy EEI measurements and the high-resolution ERB measurements, the ERB measurements need to be made with **full angular coverage**. With full angular coverage, we mean that the entire low resolution radiometer footprint is imaged with wide field of view cameras covering the entire footprint. This full angular coverage will also be beneficial for reducing the angular conversion error when converting high-resolution radiances to top-of-the-atmosphere high-resolution flux estimates. As the satellite flies over a given scene on earth, nearly simultaneous cross-track multi-angle observations of the same scene are obtained. This allows to replace the classical single angle radiance to flux conversion, by a **multi-angle radiance to flux conversion**. Using the multi-angle radiances should result in a significant reduction of the angular conversion error compared to the single radiance case.

IOP Conf. Series: Earth and Environmental Science **1522** (2025) 012019 doi:10.1088/1755-1315/1522/1/012019

The Earth Climate Observatory (ECO) mission concept was recently selected by the European Space Agency as one of the 4 candidate Earth Explorer 12 missions, that will be further studied in Phase 0 until mid 2026. The current paper provides a broad overview of the ECO mission objectives, the mission requirements, and the key elements of a baseline mission concept. During Phase 0, the ECO mission concept will be further elaborated in two parallel industrial studies, which may or may not adopt or refine the elements of the baseline concept.

2 Mission Objectives

2.1 Earth Energy Imbalance

Mission Objective 1 (MO1) of the ECO mission is the direct measurement of the global annual mean **Earth Energy Imbalance (EEI)** with high accuracy and stability.

2.2 Earth Radiation Budget mapping

Mission Objective 2 (MO2) of the ECO mission is the **high resolution** mapping of the **Reflected Solar Radiation (RSR)** and the **Outgoing Longwave Radiation (OLR) at the seasonal timescale**, with the high resolution radiances intercalibrated to the EEI measurements (MO1), and with accurate conversion of high resolution radiances to fluxes at the top of the atmosphere.

2.3 Secondary mission objectives

The following objectives provide additional benefits for the mission, but are not design drivers.

2.3.1 FORUM and TRUTHS synergy ECO will provide global monitoring of the broadband fluxes at the top of the atmosphere (MO2), tied to a Sun-Earth intercalibration of incoming and outgoing fluxes at satellite altitude. This is complementary to: 1) the **TRUTHS hyperspectral nadir reflected solar radiance** observations, independently intercalibrated to incoming solar radiation, 2) the **FORUM hyperspectral nadir emitted thermal radiance** observations, which – in synergy with IASI-NG will resolve the entire spectrum from 4 to 100-micron wavelengths.

2.3.2 Polar cap coverage Given the required full angular coverage, and 90° inclination orbits, the ECO high-resolution ERB instruments will have **extended polar cap coverage** compared to conventional meteorological imagers on polar meteorological satellites, such as AVHRR on MetOp, METimage on MetOp-SG, and VIIRS on Suomi NPP and the follow-on NOAA JPSS satellites. Thus, the ECO imagers will compliment the meteorological imagers on polar and geostationary satellites, forming a part of the so-called **ISCCP-NG** (International Satellite Cloud Climatology Project – New Generation).

2.3.3 Stereo vision and Atmospheric Motion Vectors Given the full angular coverage, the ECO high-resolution ERB instruments will provide good opportunities for **stereo vision** – similar to MISR, and the improved determination of **Atmospheric Motion Vectors**, in particular in the polar region, of interest to operational weather forecasting.

3 Mission requirements

3.1 Earth Energy Imbalance absolute accuracy and stability requirements

The EEI needs to be measured with a threshold absolute accuracy of 1.4 W/m^2, and a threshold stability of 0.3 W/m^2dec, a goal absolute accuracy of 0.3 W/m^2, and a goal stability of 0.1 W/m^2dec. The absolute accuracy is understood as a bias, and the stability is understood as a slow drift of this bias [Ohring et al., 2005]. These requirements are derived from the Global Climate Observing System (GCOS) of the World Meteorological Organization (WMO) requirements [GCOS, 2022] on the incoming solar radiation (ISR), reflected solar radiation (RSR) and outgoing longwave radiation (OLR), which are based on [Ohring et al., 2005]. If the errors on the ISR, RSR and OLR are uncorrelated, we can derive the required error on the EEI as the square root of the sum of squares.

3.2 Earth Energy Budget broadband regression error

In contrast to existing broadband radiometers, for ECO we choose to derive the Earth Radiation Budget (ERB) terms from wide field of view cameras. Advantages of this ECO approach are:

1. Full angular coverage of the field of view of the radiometer, and thus the possibility to transfer the high radiometric accuracy and stability of the radiometer to the cameras.
2. A strong reduction of the angular conversion error - which is the dominant error source in the case of single view broadband radiometers.

As a threshold requirement, the camera broadband regression errors should not be larger than the demonstrated absolute accuracy of existing broadband radiometers. Following [Dewitte and Clerbaux, 2017], these demonstrated accuracies and hence ECO threshold broadband regression error requirements are 2.7% for the RSR, and 0.84% for the OLR.

3.3 Earth Energy Budget spatial resolution

Since the presence of clouds is the most important variable parameter influencing the Earth Outgoing Radiation, as a threshold requirement the spatial resolution of the cameras should be high enough to discriminate sufficiently between cloudy and clear sky scenes. In addition, in order to obtain a scene identification as used for the definition of the state of the art CERES/MODIS Angular Dependency Models, as a goal a spatial resolution comparable to MODIS is desirable.

We adopt as a threshold Ground Sampling Distance (GSD) 5 km at nadir, and as a goal GSD 1 km at nadir. As a goal the threshold GSD of 5 km should be met over the entire swath width of 2550 km needed for a full earth coverage.

4 Key elements of baseline mission concept

4.1 Description of the observation technique and instrument concepts

The principle of measuring EEI is to define a surface surrounding the Earth where the difference between the incoming and outgoing fluxes is evaluated. In an idealized scenario, the simplest solution would be to place this virtual control surface at the satellite level, a concept that has been shown to work from first principles using perfect cosine response radiometers with 180 degree field of view [Mishchenko et al., 2016]. Technically, however, it is difficult to design such an idealised radiometer with high accuracy at large viewing angles.

Instead, for ECO, as in earlier missions, a baffle is used to limit the view angle to a virtual control surface which is situated closer to Earth (Figure 1). In order to use this approach it is necessary to place the control surface sufficiently high above the Earth's surface so that interference is negligible, i.e. absorption, scattering or emission in the thin atmosphere above the control surface and below the satellite can be ignored. In this way, the global mean outgoing flux observed at the satellite level is the same as that emanating at the control surface. The incoming solar radiation can then be calculated as the product of the measured total solar irradiance, and the solar-exposed cross section of the control surface. The outgoing flux is comprised of emitted terrestrial radiation, reflected sunlight, as well as transmitted sunlight observed by the radiometer during twilight situations (example in Figure 1, left).

The virtual control surface height is determined by the view angle of the radiometer and the satellite orbit altitude. The current choice is to place the control surface around 100 km above the equatorial Earth surface, which for the case of a 700 km average orbit altitude corresponds to a field of view from limb to limb of approximately 132 degrees. This choice will be confirmed or adjusted in Phase 0.

The ECO satellite payload is based on an innovative self-calibrating concept with four identically designed radiometers, flanked by a complementary suite of cameras, C_s and C_l, to measure the spatial distribution of the shortwave and longwave outgoing radiation (Figure 1, right). Two radiometers will be placed on the zenith face of the satellites, viewing space and the Sun, and two at the nadir face pointing at the Earth. The radiometers can be intercalibrated in orbit by rotating the satellites upside down. This is vital for measuring EEI which is

IOP Conf. Series: Earth and Environmental Science **1522** (2025) 012019 doi:10.1088/1755-1315/1522/1/012019

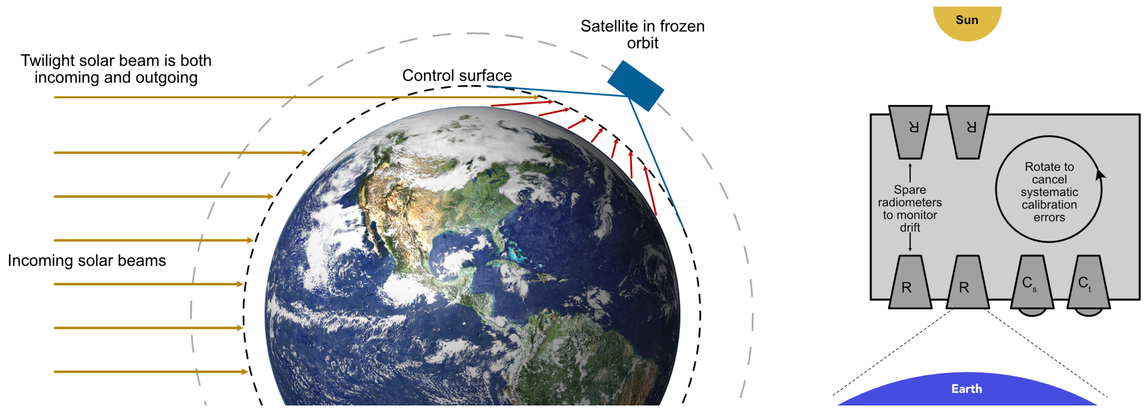

Figure 1: Viewing geometry for a WFOV mission is shown on the left. The virtual control surface defines the incoming and outgoing terms. Solar beams are shown in yellow and terrestrial emitted radiation in red. In general, there will also be reflected sunlight observed by the nadir radiometers. The illustration is not drawn to scale. On the right the general conceptual layout of an ECO satellite payload is shown.

the difference of two absolute measurements. In addition, by having dual radiometers sitting side-by-side on either side of the satellite, it is possible to monitor and correct for drifts in the radiometer sensitivity over time by keeping one of them closed and protected most of the time.

The camera suites will provide the directional distribution of the outgoing reflected sunlight and emitted terrestrial radiance. The cameras will have sufficient spectral channels to allow a statistical reconstruction of the broadband radiation with low broadband regression error. The uncooled cameras will be equipped with shutters providing a stand alone in-flight calibration capability. The final calibration of the camera derived high resolution broadband radiances will be obtained from cross-calibration with the radiometer. From the multi-angle multi-spectral camera radiances high resolution RSR and OLR fluxes will be derived to serve Mission Objective 2 (MO2).

The current state of the art for high resolution ERB flux estimation is to estimate the ERB fluxes from single view radiances through detailed scene identification and empirical Angular Dependency Models (ADMs) [Loeb et al., 2003]. In this approach, the estimated 2 sigma errors are 20 W/m^2 for the RSR and 10 W/m^2 for the OLR [Loeb et al., 2007]. For ECO, we aim to develop new flux estimation algorithms, where the flux is estimated from multi-angle radiances, which should lead to a significant reduction of the flux estimation errors.

4.1.1 Wide field of view radiometer The well proven observation principle of the ECO radiometer is to expose a surface element of known size – the precision aperture – to allow incident radiant flux from the Earth or the Sun to enter a highly absorbing cavity where it can be quantified (Figure 2). The ECO radiometer measures this flux using the electrical substitution principle: a shutter opens and closes the precision aperture opening while a thermal control system applies heating to keep the cavity at a constant temperature. The applied difference in heating power is then the difference in incoming flux between the open and closed states. This principle of operation was used in the PMOD6 [Fröhlich et al., 1995, Finsterle et al., 2021] and DIARAD [Dewitte et al., 2004] as part of the VIRGO instrument package aboard the SOHO satellite observing the total solar irradiance since 1996 and numerous subsequent absolute radiometers, such as PREMOS onboard PICARD [Schmutz et al., 2009], DARA/JTSIM onboard FY3-E [Montillet et al., 2023], CLARA/NorSat-1 [Walter et al., 2017, Haberreiter et al., 2023] as well as DARA/PROBA3 to be launched end of 2024.

In contrast, ERBE mission instead applied dual cavities, one facing out of and the other facing into the instrument casing, without the use of a shutter, a concept that caused major issues with thermal offsets [Wong et al., 2018].

The interior of the cavity is covered with a highly absorptive black paint, the Nextel 811-21 black coating [Adibekyan et al., 2017] was adopted as a baseline, since it has a long space heritage for solar radiometers, it

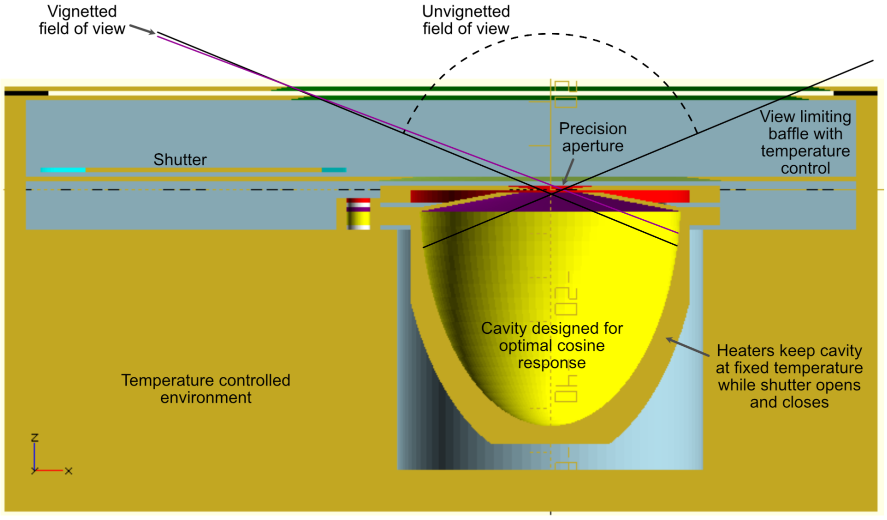

Figure 2: Wide field of view radiometer design for the ECO mission.

can be applied to curved surfaces, and it has been shown to preserve absorptivity well into the far infrared. The shape of the cavity is designed such that absorption dependency on the incident angle is minimised, and we estimate an uncertainty arising from varying incident angles of just 240 ppm, or equivalently 0.08 Wm^{-2}. This choice is different from earlier designs that instead prioritised optimisation of total absorption by funneling the reflected photons deeper and deeper into the cavity [Kendall, 1969, Willson, 1973, Barkstrom and Smith, 1986, Swartz et al., 2019]. In the ECO mission we prioritise being able to measure the difference between incoming and outgoing, and hence the EEI. The total absorption of the cavity, despite prioritising an improved cosine response, is high. For the nominal Nextel 811-21 black coating reflectance of 3 percent, only 0.25 percent of the reflected light escapes through the precision aperture due to multiple reflection inside the instrument cavity. Thus, 99.9975 percent is eventually absorbed within the cavity. The spectral flatness of the cavity absorption is better than 0.01 percent. The deviation from a perfect cosine angular response is better than 0.0015 percent.

Anything placed in front of the precision aperture can cause emission, reflections and scattering that will disturb the measurement. The view limiting baffle is designed to minimise these effects. The baffle is designed along the lines of a blackbody calibration source [Mason et al., 1996]: it is thermally isolated from its surrounding, in order to maximise its thermal uniformity, and its temperature is measured. Similar to [Mason et al., 1996], we will assume that we can reach a temperature uniformity and knowledge of the baffle temperature of 0.1 K. An error of 0.1 K on the baffle temperature corresponds to an error of 0.31 Wm^{-2} on the baffle thermal emission, which is used in the error calculations that follow. In addition all slanted edges are on the underside to avoid reflections into the precision aperture. The exception is the aperture itself. Here it must be ensured that the angle of the edge does not permit incoming radiation to be reflected into the cavity (Figure 2). Finally, scattering from the baffle edge into the cavity is reduced by increasing the baffle size compared to earlier designs [Schifano et al., 2020b], whereby it can be shown that scattering decreases inversely proportionally to the baffle radius. The baffle radius can be further increased if needed.

An additional advantage of the enlarged view limiting baffle is that the vignetted field of view, which is a range of angles wherein the precision aperture is partially shaded by the baffle, becomes smaller (Figure 2). The vignetted field of view depends on the size of the baffle and the aperture and in the presented design it is less than 2 degrees. When the Sun is within the vignetted field of view during twilight situations (Figure 1) the response will be damped and this must be taken into account. In a noon-midnight orbit this affects about 1 percent of the data. In our accuracy estimates we conservatively adopt the corresponding error estimate for the ERBE mission from Wong et al. [2018].

The sensitivity of this type of radiometer is known to decrease slowly over time, mainly because the absorptivity of the cavity decreases when the black paint is exposed to solar UV light. This issue is minimised using a dual radiometer setup with one operating and one spare radiometer on each side of the ECO satellite. The spare radiometers will be protected with the shutter when not operated. This same principle was used for the very similar DIARAD instrument on SOHO measuring the total solar irradiance. By only occasionally operating the spare instrument it was possible to determine that the main instrument lost sensitivity corresponding to about 1.5 Wm^{-2} of approximately 1360 Wm^{-2} in 25 years. If converted to the 340 Wm^{-2} signals we will measure for ECO this corresponds to approximately 0.2 Wm^{-2} per decade anticipated drift, in between the ECO Mission treshold and goal requirement (Section 3). Furthermore, this drift can be monitored and corrected for by use of the spare radiometers. For instance if these are used during 1/1000 of the time, then the drift can be reduced by a similar magnitude. Hence, we expect the ECO mission is able to meet and exceed the goal stability requirement with considerable margin.

In summary, **the ECO mission radiometers are improved in a number of ways compared to earlier missions, in particular ERBE, but at the same time are based on well known and space proven technology.**

4.1.2 Radiometer accuracy estimate The accuracy of the Sun-Earth intercalibration by the WFOV radiometer is estimated to be 0.38 W/m^2, with details given in table 1. **The baffle thermal emission error is the dominant error source**, as it also was for the ERBE WFOV radiometer [Wong et al., 2018]. It occurs twice, once for the incoming solar radiation, and once for the outgoing terrestrial radiation.

Total	989 ppm = 0.34 W/m^2
RMS	**1119 ppm = 0.38 W/m^2**
Baffle thermal emission	**915 ppm = 0.31 W/m^2**
Twilight data	588 ppm = 0.2 W/m^2
Position dependence	240 ppm = 0.08 W/m^2
Electrical power	100 ppm = 0.03 W/m^2
Cavity absorption	13 ppm = 0.004 W/m^2

Table 1: Radiometer Sun-Earth intercalibration accuracy estimate.

The accuracy of the global annual mean EEI is estimated to be **0.41 W/m^2**, with details given in table 2.

Total	2327 ppm = 0.79 W/m^2
RMS	**1213 ppm = 0.41 W/m^2**
Sun-Earth intercalibration	1119 ppm = 0.38 W/m^2
Diurnal cycle sampling (2 satellites)	470 ppm = 0.16 W/m^2

Table 2: ECO EEI accuracy estimate.

5 Shortwave camera suite

The shortwave camera suite refers to the cameras operating in the visible to near-infrared (VNIR) spectral range, for which possible reference designs have been presented in [Schifano et al., 2020a] and [Dewitte et al., 2023]. These designs feature a CMOS Si detector arrays with a wide field of view lens enabling a view of the Earth from limb to limb. The detector size in [Dewitte et al., 2023] is 3000x3000 pixels, with nadir pixel resolution of 0.57 km.

Following [Schifano et al., 2020a], the RSR can be estimated on a stand-alone basis from an RGB CMOS imager through spectral regression with the error due to the broadband regression of 3%. These results are comparable with those of [Loeb et al, 2006] where an empirical broadband regression of the RSR from the MISR blue (446 nm), red (672 nm) and near-infrared (867 nm) radiances was trained with CERES data, with a broadband regression error of 4%.

We note that using only a Si detector, with sensitivity below 1000 nm, the required broadband regression error of 2.7% can not be achieved. This can be understood, since below 1000 nm bright scenes such as water clouds, ice clouds and snow, can have a similar reflection – dependent on optical depth, while at ShortWave InfraRed (SWIR) wavelengths, they have a very different absorption - dependent on particle size [Nakajima and King, 1990], [Jin et al., 2008]. In order to capture the missing information not captured with a Si detector, a SWIR or a VIS-SWIR channel using an InGaAs detector needs to be added. The highest spatial resolution and widest spectral response that is available COTS uses the Sony SenSWIR$^{\mathrm{TM}}$ technology.

We therefore propose as a new reference design, a system with two cameras, one RGB CMOS Si camera with a detector size 3000x3000, and one uncooled Sony SenSWIR$^{\mathrm{TM}}$ camera with a detector size 1500x1500, to provide the required VIS-SWIR, Red, Green, Blue spectral bands at a resolution close to 1 km at nadir. The spectral responses are illustrated in figure 3. The estimated RSR broadband regression error is 0.5 %, well below the required 2.7 %. The updated RSR broadband regression will be described in more detail in a separate paper. The spectral bands also allow the required scene type discrimination between water clouds, ice clouds, clear sky ocean, coarse (natural) and fine (anthropogenic) aerosols over ocean, vegetated land, desert, snow/ice.

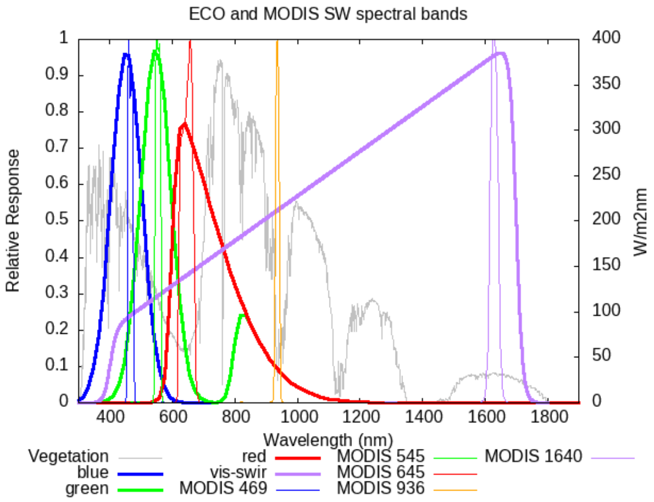

Figure 3: RGB CMOS Si and VIS-SWIR InGaAs spectral responses

We consider a quadratic law

$$\theta = k1 * p + k2 * p^2 \tag{1}$$

where through the choice of the constants $k1$ and $k2$ independently the nadir GSD, and the total field of view can be chosen. For a detector of 1000^2 pixels, a satellite altitude of 700 km, and a half field of view size of $67.2°$, the quadratic laws for GSDs of 1, 2, 2.8 and 3.1 km are illustrated in figure 4.

The corresponding GSDs as a function of the distance to the nadir point are illustrated in figure 5.

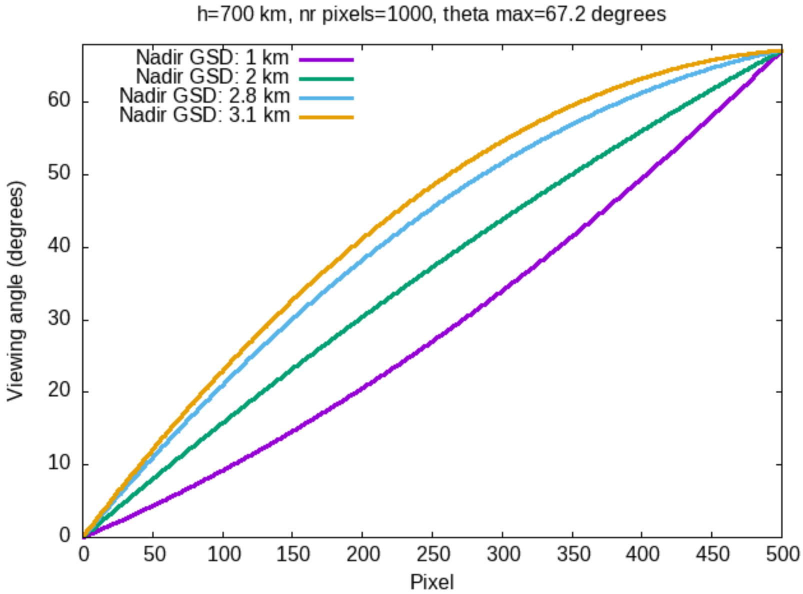

Figure 4: Quadratic laws for lens viewing angle.

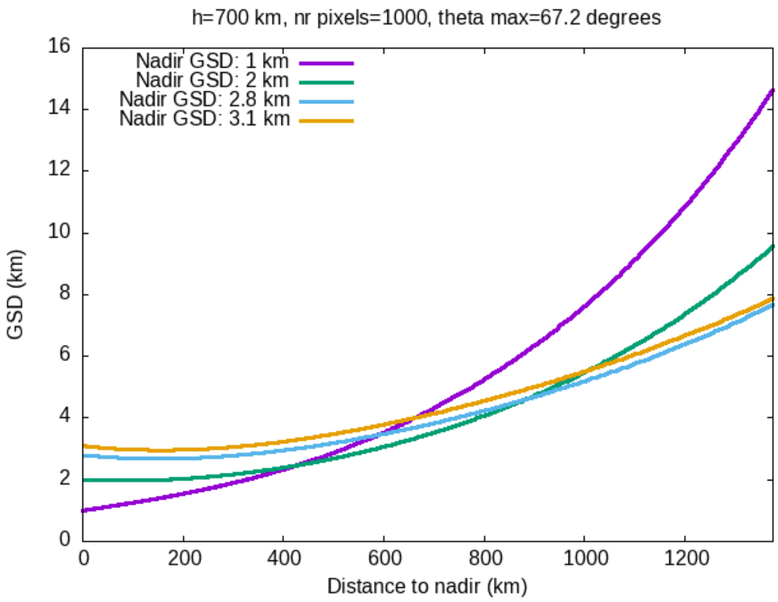

Figure 5: Ground Sampling Distance for quadratic lenses.

In order to have full coverage of the Earth at the equator, a swath width of approximately 2550 km is needed. The edge of this swath is located at 1275 km from the nadir point. In the first four rows of table 3, the nadir and the edge GSD - taken at 1275 km from the nadir point - of the lens designs of figures 4 and 5 are listed. A minimal edge GSD of 7.7 km is obtained for the design with a nadir GSD of 2.8 km. Scaling the lens with nadir/edge GSD of 2.8/7.7 km for a 1000^2 detector, results in a nadir/edge GSD of 1.9/5.1 km for a 1500^2 detector, and 0.9/2.6 km for a 3000^2 detector.

Pixels	Nadir GSD (km)	Edge GSD (km)
1000	1	14.6
1000	2	9.5
1000	**2.8**	**7.7**
1000	3.1	7.9
1500	**1.9**	**5.1**
3000	**0.9**	**2.6**

Table 3: Nadir and Edge Ground Sampling Distance for different lens designs.

The only on-board calibration source for the shortwave camera suite will be a shutter, allowing verification of the dark current, and also shielding the camera from direct solar illumination during solar pointing. The camera spectral gains and dark current will be determined pre-flight during ground calibration. The stability of the RGB spectral responses and the gains will be monitored, and if needed adjusted in-flight through vicarious calibration monitoring stable Earth targets similar to [Wu et al., 2012], [Decoster et al., 2014], [Sterckx et al., 2016].

Since broadband spectral bands are proposed, plenty of photons are available, allowing a SNR with ample margin compared to the requirement, as verified in [Dewitte et al., 2023] for the RGB CMOS camera. We expect similar results for the InGaAs camera, and therefore we also expect that is not necerssary to cool the InGaAs camera. An **uncooled** InGaAs camera is preferred for low ageing, high thermal stability of the radiometer, and low power and weight.

6 Longwave camera suite

The longwave cameras are thermal infrared imagers of which reference designs are described in [Schifano et al., 2021]. It features the same wide field of view of the shortwave camera, but uses a microbolometer detector array. The nadir sampling distance is 2 km, for a detector size of 750x750 pixels. Using a single wavelength band of 8-14 micron, the OLR can be estimated on a stand-alone basis from the thermal imager with an error due to the broadband regression of 5%.

The longwave cameras will be equipped with a shutter with known temperature and known high emissivity. This shutter will act as a flat blackbody. Combined with the deep space view a two-point in-flight calibration for the longwave cameras will be implemented. The shutter view will be used for the characterisation of the thermal offset as a function of the lens temperature. The deep space view will be used for an in-flight verification of the gain, which will also be measured on the ground before flight.

To improve the OLR spectral regression noise, the number of ECO longwave channels can be increased. This will be done by using multiple cameras, with filters inserted in front of the microbolometer detector array. In [Okada et al., 2022], the TIRI/HERA space instrument is described using the same detector as in [Schifano et al., 2021], and a filter wheel with 6 filters each having a bandwidth of approximately 1 μm. For ECO we will adopt similar filters WV_7.7, Cloud_8.55, O3_9.7, Cloud_10.85, Cloud_11.9, CO2_12.9, listed in table 4.

The 6 ECO filter spectral responses are also similar to filter responses used for the SEVIRI/MSG and FCI/MTG instruments.

The ECO LW Camera Suite will be formed by 6 separate longwave cameras, each consisting of the same microbolometer array and wide field of view lens, and each equiped with a different filter realising the spectral response from table 4.

The LW spectral responses are illustrated in figure 6.

Band	Limits
WV_7.7	6-8 μm
Cloud_8.55	8-9.1 μm
O3_9.7	9.1-10.3 μm
Cloud_10.85	10.3-11.4 μm
Cloud_11.9	11.4-12.5 μm
CO2_12.9	12.5-14 μm

Table 4: ECO longwave spectral bands.

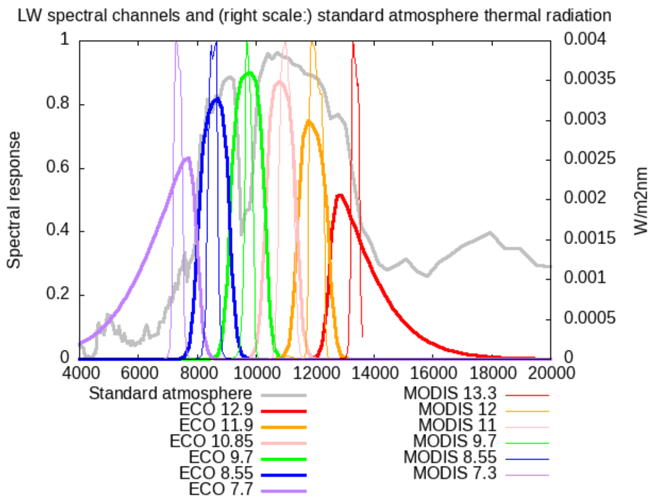

Figure 6: Longwave spectral responses.

It is expected that with the use of these 6 LW cameras, the OLR can be estimated on a stand-alone basis with a broadband regression error of 0.6 %. Considering a 1000x1000 microbolometer detector array, and the optimal quadratic lens design of table 3, a nadir/edge GSD of 2.8/7.7 km can be achieved.

Concerning NEDT, in [Dewitte et al., 2023], it was estimated that there is an ample margin compared to the requirement. We expect similar results for the updated ECO baseline concept.

7 Summary

The ECO space mission concept is currently in Phase 0 as a candidate ESA Earth Explorer 12 candidate. The primary mission objectives of the ECO mission are:

1. to measure the Earth Energy Imbalance directly from space at the annual mean timescale, with unprecedented accuracy and stability.
2. to provide enhanced continuity of the high resolution monitoring of the Earth Radiation Budget terms of Outgoing Longwave Radiation and Reflected Solar Radiation.

The current baseline ECO concept consists of two identical satellites, in orthogonal 90° inclination orbits. Following the simulation results of [Hocking et al., 2024], the global annual mean EEI can be measured with such a constellation with an annual mean sampling error of 0.16 W/m^2. During Phase 0 the science team will also investigate other orbit configurations.

Each satellite is equipped with 2 pairs of identically designed wide field of view radiometers. The nominally nadir viewing pair of radiometers assures the observation of the Total Outgoing Radiation at satellite altitude. The nominally zenith viewing pair of radiometers assures the observation of the Incoming Solar Radiation at satellite altitude. Periodically, the satellite will be rotated by 180° degrees for Sun-Earth intercalibration. Incoming and outgoing radiation is defined by a reference surface, which by default will be a sphere located at 100 km above the equatorial Earth radius. For each pair of radiometers, one radiometer is observing continuously, the second one is a backup radiometer with low exposure to solar UV radiation, to allow ageing to be monitored and corrected. The radiometers are electrical substitution cavity radiometers, with long heritage from Total Solar Irradiance observation.

The estimated accuracy of the global annual mean EEI is 0.41 W/m^2, with as dominant error source the radiometer baffle thermal emission. This dominant error source can be reduced by reducing the emissivity of the baffle.

High resolution observation of the Reflected Solar Radiation and Outgoing Longwave Radiation will be made by shortwave and longwave camera suites. Providing multispectral observations from a pixel arrays that will enable the broadband RSR and OLR to be estimated with a regression error of 0.5% and 0.6% respectively.

The full angular coverage of the cameras, combined with their spectral information, is expected to allow a strong reduction of the angular radiance to flux conversion error compared to the state of the art [Loeb et al., 2003], which is based on the radiance to flux conversion for single radiance views.

The current paper presents the ECO mission justification, the main requirements, and a baseline ECO space mission concept. Two parallel Phase 0 industrial studies will be conducted to further mature the ECO mission concept.

References

A. Adibekyan, E. Kononogova, C. Monte, and J. Hollandt. High-accuracy emissivity data on the coatings nextel 811-21, herberts 1534, aeroglaze z306 and acktar fractal black. *International Journal of Thermophysics*, 38(6): 1–14, 2017.

R. Alfaro-Contreras, J. Zhang, J.S. Reid, and S. Christopher. A study of 15-year aerosol optical thickness and direct shortwave aerosol radiative effect trends using modis, misr, caliop and ceres. *Atmospheric Chemistry and Physics*, 17(22):13849–13868, 2017.

B. R. Barkstrom and G. L. Smith. The earth radiation budget experiment: Science and implementation. *Rev. Geophys.*, 24(2):379–390, 1986.

I. Decoster, N. Clerbaux, E. Baudrez, S. Dewitte, A. Ipe, S. Nevens, A.V. Blazquez, and J. Cornelis. Spectral aging model applied to meteosat first generation visible band. *Remote Sensing*, 6(3):2534–2571, 2014.

S. Dewitte and N. Clerbaux. Measurement of the earth radiation budget at the top of the atmosphere—a review. *Remote Sensing*, 9(11):1143, 2017.

S. Dewitte, D. Crommelynck, and A. Joukoff. Total solar irradiance observations from diarad/virgo. *Journal of Geophysical Research: Space Physics*, 109:A2, 2004.

S. Dewitte, N. Clerbaux, and J. Cornelis. Decadal changes of the reflected solar radiation and the earth energy imbalance. *Remote Sensing*, 11(6):663, 2019.

S. Dewitte, A.A. Abdul Nazar, Y. Zhang, and L. Smeesters. A multispectral camera suite for the observation of earth's outgoing radiative energy. *Remote Sensing*, 15(23):5487, 2023.

D.R. Doelling, D.F. Keyes, M.L. Nordeen, D. Morstad, C. Nguyen, B.A. Wielicki, D.F. Young, and K. Sun. Geostationary enhanced temporal interpolation for ceres flux products. *J. Atmos. Oceanic Technol.*, 30(6): 1072–1090, 2013. doi: 10.1175/JTECH-D-12-00136.1.

W. Finsterle, J. P. Montillet, W. Schmutz, R. Šikonja, L. Kolar, and L. Treven. The total solar irradiance during the recent solar minimum period measured by SOHO/VIRGO. *Scientific Reports*, 11:7835, January 2021. doi: 10.1038/s41598-021-87108-y.

C. Fröhlich, J. Romero, H. Roth, C. Wehrli, B. N. Andersen, T. Appourchaux, V. Domingo, U. Telljohann, G. Berthomieu, P. Delache, J. Provost, T. Toutain, D. A. Crommelynck, A. Chevalier, A. Fichot, W. Dappen, D. Gough, T. Hoeksema, A. Jimenez, M. F. Gomez, J. M. Herreros, T. R. Cortes, A. R. Jones, J. M. Pap, and R. C. Willson. VIRGO: Experiment for Helioseismology and Solar Irradiance Monitoring. , 162:101–128, 1995.

WMO GCOS. *The 2022 GCOS ECVs Requirements (GCOS-245).* 2022.

Margit Haberreiter, Wolfgang Finsterle, Jean-Philippe Montillet, Manfred Gyo, Dany Pfiffner, Martin Mostad, Ivar Spydevold, Alex Beattie, Bo Andersen, and Werner Schmutz. Total Solar Irradiance and Terrestrial Outgoing Longwave Radiation Measurements obtained with CLARA onboard NorSat-1. In *EGU General Assembly Conference Abstracts*, EGU General Assembly Conference Abstracts, pages EGU–7221, 2023. doi: 10.5194/egusphere-egu23-7221.

J. Hansen, L. Nazarenko, R. Ruedy, M. Sato, J. Willis, A. Del Genio, D. Koch, A. Lacis, K. Lo, S. Menon, and T. Novakov. Earth's energy imbalance: Confirmation and implications. *Science*, 308(5727):1431–1435, 2005.

D.L. Hartmann and P. Ceppi. Trends in the ceres dataset, 2000–13: The effects of sea ice and jet shifts and comparison to climate models. *Journal of Climate*, 27(6):2444–2456, 2014.

T. Hocking, T. Mauritsen, and L. Megner. Sampling the diurnal and annual cycles of the earth's energy imbalance with constellations of satellite-borne radiometers. *EGUsphere*, 2024-356:1–25, 2024.

IPCC. The earth's energy budget, climate feedbacks, and climate sensitivity. *Climate Change 2021: The Physical Science Basis. Contribution of Working Group I to the Sixth Assessment Report of the Intergovernmental Panel on Climate Change*, pages 923–1054, 2021. doi: 10.1017/9781009157896.009.

Z. Jin, T.P. Charlock, P. Yang, Y. Xie, and W. Miller. Snow optical properties for different particle shapes with application to snow grain size retrieval and modis/ceres radiance comparison over antarctica. *Remote Sensing of Environment*, 112(9):3563–3581, 2008.

S. Kato, N. Loeb, F. Rose, T. Thorsen, D. Rutan, S.H. Ham, and D. Doelling. Earth radiation budget climate record composed of multiple satellite observations. In XXVIII General Assembly of the International Union of Geodesy and Geophysics (IUGG), July 2023.

Y.J. Kaufman, O. Boucher, D. Tanré, M. Chin, L.A. Remer, and T. Takemura. Aerosol anthropogenic component estimated from satellite data. *Geophysical Research Letters*, 32(17), 2005.

J.M. Kendall. Primary absolute cavity radiometer. Technical Report JPL-TR-32-1396, 1969.

N. G. Loeb, N. Manalo-Smith, S. Kato, W. F. Miller, S. K. Gupta, P. Minnis, and B. A Wielicki. Angular distribution models for top-of-atmosphere radiative flux estimation from the clouds and the earth's radiant energy system instrument on the tropical rainfall measuring mission satellite. part i: Methodology. *Journal of applied meteorology*, 42(2):240–265, 2003.

N. G. Loeb, S. Kato, K. Loukachine, N. Manalo-Smith, and D. R. Doelling. Angular distribution models for top-of-atmosphere radiative flux estimation from the clouds and the earth's radiant energy system instrument on the terra satellite. part ii: Validation. *Journal of Atmospheric and Oceanic Technology*, 24(4):564–584, 2007.

N.G. Loeb, D.R. Doelling, H. Wang, W. Su, C. Nguyen, J.G. Corbett, L. Liang, C. Mitrescu, F.G. Rose, and S. Kato. Clouds and the earth's radiant energy system (ceres) energy balanced and filled (ebaf) top-of-atmosphere (toa) edition-4.0 data product. *Journal of Climate*, 31(2):895–918, 2018.

I.M. Mason, P.H. Sheather, J.A. Bowles, and G. Davies. Blackbody calibration sources of high accuracy for a spaceborne infrared instrument: the along track scanning radiometer. *Applied optics*, 35(4):629–639, 1996.

A. Minière, K. von Schuckmann, J.B. Sallée, and L. Vogt. Robust acceleration of earth system heating observed over the past six decades. *Scientific Reports*, 13(1):22975, 2023.

M.I. Mishchenko, J.A. Lock, A.A. Lacis, L.D. Travis, and B. Cairns. First-principles definition and measurement of planetary electromagnetic-energy budget. *JOSA A*, 33(6):1126–1132, 2016.

Jean-Philippe Montillet, Wolfgang Finsterle, Ping Zhu, and et al. Assessment of solar variability through the analysis of tsi observations recorded by the fy3e/jtsim/dara radiometer. ESS Open Archive, December 2023.

T. Nakajima and M.D. King. Determination of the optical thickness and effective particle radius of clouds from reflected solar radiation measurements. part i: Theory. *J. Atmos. Sci*, 47(15):1878–1893, 1990.

G. Ohring, B. Wielicki, R. Spencer, B. Emery, and R. Datla. Satellite instrument calibration for measuring global climate change: Report of a workshop. *Bulletin of the American Meteorological Society*, 86(9):1303–1314, 2005.

T. Okada, S. Tanaka, N. Sakatani, Y. Shimaki, T. Arai, H. Senshu, H. Demura, T. Sekiguchi, T. Kouyama, M. Kanamaru, and T. Ishizaki. Calibration of the thermal infrared imager tiri onboard hera. pages EPSC2022–1191. In European Planetary Science Congress, September 2022.

L. Schifano, L. Smeesters, F. Berghmans, and S. Dewitte. Optical system design of a wide field-of-view camera for the characterization of earth's reflected solar radiation. *Remote Sensing*, 12(16):2556, 2020a.

L. Schifano, L. Smeesters, T. Geernaert, F. Berghmans, and S. Dewitte. Design and analysis of a next-generation wide field-of-view earth radiation budget radiometer. *Remote Sensing*, 12(3):425, 2020b.

L. Schifano, L. Smeesters, F. Berghmans, and S. Dewitte. Wide-field-of-view longwave camera for the characterization of the earth's outgoing longwave radiation. *Sensors*, 21(13):4444, 2021.

W. Schmutz, A. Fehlmann, G. Hülsen, P. Meindl, R. Winkler, G. Thuillier, P. Blattner, F. Buisson, T. Egorova, W. Finsterle, N. Fox, J. Gröbner, J.-F. Hochedez, S. Koller, M. Meftah, M. Meisonnier, S. Nyeki, D. Pfiffner, H. Roth, E. Rozanov, M. Spescha, C. Wehrli, L. Werner, and J. U. Wyss. The PREMOS/PICARD instrument calibration. *Metrologia*, 46:202–+, August 2009. doi: 10.1088/0026-1394/46/4/S13.

S. Sterckx, S. Adriaensen, W. Dierckx, and M. Bouvet. In-orbit radiometric calibration and stability monitoring of the proba-v instrument. *Remote Sensing*, 8(7):546, 2016.

W. Swartz, S. Lorentz, S. Papadakis, P. Huang, A. Smith, D. Deglau, Y. Yu, S. Reilly, N. Reilly, and D. Anderson. Ravan: Cubesat demonstration for multi-point earth radiation budget measurements. *Remote Sensing*, 11:796, 2019. doi: 10.3390/rs11070796.

K.E. Trenberth, J.T. Fasullo, K. Von Schuckmann, and L. Cheng. Insights into earth's energy imbalance from multiple sources. *Journal of Climate*, 29(20):7495–7505, 2016.

UN. *Framework Convention on Climate Change: Adoption of the Paris Agreement.* 21st Conference of the Parties, Paris, 2016.

K. Von Schuckmann, M.D. Palmer, K.E. Trenberth, A. Cazenave, D. Chambers, N. Champollion, J. Hansen, S.A. Josey, N. Loeb, P.P. Mathieu, and B. Meyssignac. An imperative to monitor earth's energy imbalance. *Nature Climate Change*, 6(2):138–144, 2016.

K. Von Schuckmann, L. Cheng, M.D. Palmer, J. Hansen, C. Tassone, V. Aich, S. Adusumilli, H. Beltrami, T. Boyer, F.J. Cuesta-Valero, and D. Desbruyères. Heat stored in the earth system: where does the energy go? *Earth System Science Data*, 12(3):2013–2041, 2020.

Benjamin Walter, Pierre-Luc Levesque, Greg Kopp, Bo Andersen, Ivo Beck, Wolfgang Finsterle, Manfred Gyo, Karl Heuerman, Silvio Koller, Nathan Mingard, Alberto Remesal Oliva, Daniel Pfiffner, Ricco Soder, Marcel Spescha, Markus Suter, and Werner Schmutz. The CLARA/NORSAT-1 solar absolute radiometer: instrument design, characterization and calibration. *Metrologia*, 54(5):674, 2017. doi: 10.1088/1681-7575/aa7a63.

R.C. Willson. Active cavity radiometer. *Applied Optics*, 12(4):810–817, 1973.

T. Wong, G. L. Smith, S. Kato, N. G. Loeb, G. Kopp, and A. K. Shrestha. On the lessons learned from the operations of the erbe nonscanner instrument in space and the production of the nonscanner toa radiation budget data set. *IEEE Transactions on Geoscience and Remote Sensing*, 56(10):5936–5947, 2018.

A. Wu, X. Xiong, D.R. Doelling, D. Morstad, A. Angal, and R. Bhatt. Characterization of terra and aqua modis vis, nir, and swir spectral bands' calibration stability. *IEEE Transactions on Geoscience and Remote Sensing*, 51(7):4330–4338, 2012.